Journal of Power Sources 242 (2013) 527–532

Contents lists available at SciVerse ScienceDirect

Journal of Power Sources

journal homepage: www.elsevier.com/locate/jpowsour

Sn–O–C composite anode for Li secondary battery synthesized by an electrodeposition technique using organic carbonate electrolyte

Toshiyuki Momma [a,b], Moongook Jeong [a], Tokihiko Yokoshima [b], Hiroki Nara [b], Ayano Toyoda [a], Tetsuya Osaka [a,b,*]

[a] Graduate School of Advanced Science and Engineering, Waseda University, 3-4-1, Okubo, Shinjuku-ku, Tokyo 169-8555, Japan
[b] Faculty of Science and Engineering, Waseda University, 3-4-1, Okubo, Shinjuku-ku, Tokyo 169-8555, Japan

HIGHLIGHTS

- Sn–O–C composite material was electrochemically synthesized in organic electrolyte.
- Simultaneous reductions of $SnCl_2$ and electrolyte solution resulted in a Sn–O–C.
- Crystalline structure of Sn in Sn–O–C was characterized.
- Sn–O–C was revealed to have long cycling life as an anode of Li secondary battery.

GRAPHICAL ABSTRACT

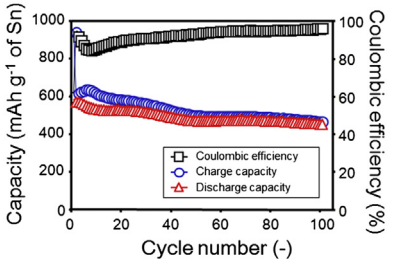

Sn-O-C composite material was successfully synthesized by the electrochemical reductions of $SnCl_2$ and electrolyte solution in organic electrolyte. Crystalline structure of Sn in the deposit was characterized and the charge-discharge cycling performance as an anode of Li secondary battery was investigated.

ARTICLE INFO

Article history:
Received 2 April 2013
Received in revised form
24 May 2013
Accepted 25 May 2013
Available online 5 June 2013

Keywords:
Tin
Anode
Sn–O–C composite
Electrodeposition
Lithium secondary battery

ABSTRACT

The Sn–O–C composite anode for the Li secondary battery was synthesized by electrodeposition using an organic carbonate solvent. The composite of Sn with organic/inorganic compounds was prepared by the simultaneous reaction of the reduction of Sn^{2+} ions and electrolysis of the mixture of ethylene carbonate and propylene carbonate. The galvanostatic potential transients for the electrodeposition of the Sn–O–C composite indicate that multiple steps of reactions corresponding to the electrochemical reduction of the tin precursor and the decomposition of organic solvents are involved. The morphology, crystalline structure and chemical composition of the as-deposited Sn–O–C composite anode were characterized to elucidate the mechanism of the synthesis of the buffering matrix enduring volume expansion.

The electrochemical behavior of the Sn–O–C composite anode was investigated by cyclic voltammetry and galvanostatical charge/discharged tests. The discharge capacity of 465 mAh (g of Sn)$^{-1}$ was obtained at the 100th cycle showing 80% of the capacity retention after the 100th cycle. The discharge capacity was stable after the 50th cycle, where the phase transformation of the Sn element from Sn to $Li_{0.4}Sn$ at the discharged state was found.

1. Introduction

Tin has been proposed as a promising element to be incorporated in the anode material ($Li_{4.4}Sn$, 994 mAh (g of Sn)$^{-1}$) for lithium secondary batteries instead of the commercial graphite anode (LiC_6, 372 mAh (g of C)$^{-1}$) to materialize an increased charge capacity of the lithium secondary battery. However, a pure tin anode suffers from a poor cycle life because of the occurrence of severe mechanical cracks and pulverization caused by significant volume expansion (~300%) during the lithiation/delithiation process [1–3]. To overcome this serious problem, various attempts, such as the use of nanostructured Sn active material [4–6], embedded matrix buffer [7–10], core–shell structure [11–13], and mesoporous structure [14–16] have been reported.

* Corresponding author. Graduate School of Advanced Science and Engineering, Waseda University, 3-4-1, Okubo, Shinjuku-ku, Tokyo 169-8555, Japan. Tel.: +81 3 5286 3202; fax: +81 3 3205 2074.
E-mail address: osakatets@waseda.jp (T. Osaka).

0378-7753/$ – see front matter © 2013 Elsevier B.V. All rights reserved.
http://dx.doi.org/10.1016/j.jpowsour.2013.05.136

Recently, many studies on Sn anodes prepared by electrodeposition techniques using aqueous solvents have been reported. The electrodeposition technique allows direct deposition of the active material onto conducting substrates; consequently, the electrodeposited anode can stand alone without employing a polymer binder. The co-deposition of Sn and nonactive inter-metallic compounds has been reported [17–22]. Furthermore, tin-based materials with carbon coating [23] or a 3D core–shell structure [24] have been prepared by an electrodeposition technique as well. Meanwhile, Sn-based anodes have been synthesized on porous Cu foam showing better cyclic performance and higher charge capacity than those deposited on a smooth Cu foil [25].

We previously investigated the electrodeposition of the Si–O–C composite anode by reducing $SiCl_4$ dissolved in polyethylene carbonate electrolyte [17,18]. The Si–O–C composite anode achieved remarkable cycling performance with outstanding durability and a high capacity of 1045 mA g^{-1} even at the 2000th charge–discharge cycle. The novel synthetic method by electrodeposition using an organic solvent makes it possible to take advantage of (i) the unnecessary nature of the polymer binder, (ii) the formation of a matrix whose chemical composition is similar to the solid electrolyte interphase (SEI) layer with permeability to Li^+ but not to electrons. The decomposition of the organic solution and the reduction of $SiCl_4$ simultaneously occurred. Consequently, the composite of Si with organic/inorganic compounds has been synthesized, which is assumed to effectively withstand the severe volume expansion.

In this study we electrodeposited an Sn–O–C composite anode using an organic solution to take advantage of the novel synthetic method examined in our previous work. It is expected that the Sn–O–C composite anode formed by the deposition of tin and the decomposition of organic solvents realizes the formation of organic/inorganic compounds, which reduces mechanical stress during the lithiation/delithiation process. In this work, we have thoroughly examined the characteristics of the electrodeposited Sn–O–C composite anode, the electrodeposition process using a new type electrolytic bath for Sn-based material, and its electrochemical performances as an anode for Li secondary batteries.

2. Experiment

The Sn–O–C composite was electrodeposited on a Ni plate substrate by a constant current deposition technique using an organic carbonate electrolytic bath. The electrolytic bath was prepared by dissolving 2.5 mmol dm^{-3} of $SnCl_2$ (Sigma–Aldrich) in an ethylene carbonate (EC): propylene carbonate (PC) (1:1 v/v) electrolyte solution (Kishida, H_2O content $<$ 20 ppm) containing 1.0 mol dm^{-3} of $LiClO_4$ which serves as a supporting electrolyte. Ni plate substrates with dimensions of 10 $\times$ 10 mm used as the working electrodes were treated in trichloroethylene and ethanol followed by an acid treatment with 10% HCl before use. A tin plate and lithium metal in glass with a Vycor chip junction served as the counter and reference electrodes, respectively. The electrodeposition cell was prepared in a glove box filled with an Ar at the dew point of below −90 °C to avoid contact with air and moisture in the atmosphere. A constant cathodic current of 37.5 μA cm^{-2} was applied to pass a charge of 0.25 C cm^{-2} for the deposition. Field emission scanning electron microscopy (FE-SEM, Hitachi S-4500S) and scanning electron microscopy (SEM, Hitachi TM-3000) equipped with an energy dispersive X-ray spectroscopy (EDS) were performed to analyze morphologies and the chemical composition of the prepared Sn–O–C composite. X-ray diffraction (XRD) was carried out by Rigaku Rint-Ultima III equipped with Cu Kα (λ = 0.1541 nm) radiation operated at 50 kV and 300 mA. The scanning range (2θ) was from 25° to 80° and the scanning speed was 3° min^{-1} using a step width of 0.02°. The electrodeposited Sn–O–C composite anode was characterized by high-resolution transmission electron microscopy (HR-TEM, H-9000UHR, Hitachi) with an accelerating voltage of 300 kV. The TEM specimens were prepared by a focused ion beam (FIB, Hitachi, FB-2000A) technique. The element depth profile was analyzed by glow discharge optical emission spectrometry (GDOES, HORIBA, JY-5000RF) with Ar sputtering in an area of 2 mm diameter. The electrochemical measurements of the prepared Sn–O–C composite anodes have been evaluated with the charge/discharge unit (Hokuto Denko HJ-1010M) using lithium half-cells fabricated with Li foils, served as a counter and reference electrode, immersed in an EC:PC (1:1 v/v) electrolyte solution (Kishida, H_2O content $<$ 20 ppm) containing 1.0 mol dm^{-3} of $LiClO_4$. The cyclic voltammetry (CV) measurement was carried out between 0.01 and 1.00 V at the scan rate of 10 mV s^{-1}. The cells were galvanostatically charged and discharged in the voltage range between 0.01 and 1.20 V vs. Li/Li^+ at the current density of 20 μA cm^{-2}.

3. Results and discussion

The electrodeposition of the Sn–O–C composite was carried out on a nickel substrate from an EC:PC electrolyte solvent containing 2.5 mmol dm^{-3} of $SnCl_2$ with 1.0 mol dm^{-3} of $LiClO_4$ used as the supporting electrolyte. Fig. 1 presents a galvanostatic potential transient during the electrodeposition of the Sn–O–C composite at 37.5 μA cm^{-2} applied with a passing charge of 0.25 C cm^{-2} for the deposition. The result reveals that the potential gradually reaches a value of 0.3 V as the deposition time is increased beyond 2500 s. The potential profile clearly shows two small and one large potential plateaus at ca. 2.2, 1.5 and 0.3 V, respectively. With the beginning of galvanostatic deposition, a rapid decrease in initial potential is followed by a small potential plateau at ca. 2.2 V. Afterward, the potential steeply reduces and reaches the stable value of ca. 1.5 V. Finally, the large plateau at ca. 0.3 V appeared after the gradual decrease in potential from 1.5 V to 0.3 V. The observed galvanostatic behavior consisting of multiple steps of potential transience may be derived from the reduction and the co-deposition of various components in the electrolytic bath, *i.e.*, Sn^{2+}, Li^+ ions and other species. Furthermore, several literature have reported that decomposition of the organic carbonate electrolyte, *i.e.*, herein EC and PC, is catalyzed by the pure tin surface, which causes SEI formation [25–27]. Therefore, it is assumed that the galvanostatic behavior indicating multiple steps of potential transients is preferable to produce the Sn–O–C composite with SEI formation by means of the co-deposition of Sn^{2+}, Li^+ ions and the decomposition of an organic carbonate electrolyte. The inset in

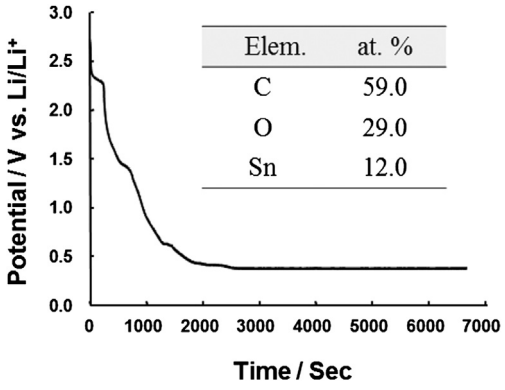

Fig. 1. The potential profile of the galvanostatic electrodeposition of Sn–O–C composite material, and the composition of the as-prepared Sn–O–C composite anode measured by EDS analysis (inset).

Fig. 1 shows the composition of the as-prepared deposits measured by EDS analysis. The result implies that the deposited composite consists of not only tin but oxygen and carbon which are decomposition products of the organic carbonate electrolyte as mentioned above. Meanwhile, the electrodeposition efficiency of a Sn element was calculated to be equal to 68% according to the elemental analysis by ICP-AES.

The surface morphology of the as-deposited Sn–O–C composite is shown in Fig. 2(a). The low-magnification SEM image indicates densely covered deposits on the substrate. However, particles with distinct shapes and sizes are irregularly deposited, forming clusters with irregular shapes. The inset shows a high-magnification image of particles with various sizes measuring from several hundred nanometers to a few micrometers. Furthermore, these particles remain inter-particle spaces resulting in micro-sized voids shown in the plane view. It appears to suggest that the existence of the space is preferable to endure pulverization of active materials by accommodating severe volume expansion during charge–discharge cycling. In Fig. 2(b), the XRD patterns of the tetragonal phase of tin are observed with peaks at 2θ values of 30.64, 32.02, 43.88, 55.34, 62.54, 63.79, 64.59 and 73.17, which are assigned to the 200, 101, 220, 301, 112, 400, 321 and 411 crystal planes (JCPDS # 04-0673), respectively.

The structure of the as-deposited Sn–O–C composite was investigated by a cross-sectional TEM image, which is shown in Fig. 3(a). The specimen preparation for TEM investigation was performed with the FIB technique. Agglomerated Sn particles with irregular shapes and different sizes are observed as dark areas. As mentioned in regards to the SEM image, the cross-sectional view of TEM also indicates the inter-particle space with the depth of ~700 nm (not completely shown), which is distinguishable as bright parts in Fig. 3(a), which presumably operates on the efficient endurance of the volume expansion of tin. Meanwhile, Fig. 3(b) shows an HR-TEM image of the 'part 1' highlighted with a dashed line in Fig. 3(a). The dark area indicates a lattice fringe of the (200) planes corresponding to the *d* space value of 2.9 Å of the tetragonal tin. Furthermore, it is clearly observed that the gray part possesses an amorphous phase surrounding Sn particles. It was produced from the decomposed organic carbonate electrolyte similar to the SEI formation. Fig. 3(c) shows the fast Fourier transformed (FFT) image of indicated as 'point 2' in Fig. 3(a). All electron diffraction images in the FFT pattern provide evidence of a body-centered tetragonal Sn structure in [001] orientation. This result shows a good agreement with the XRD pattern in Fig. 2(b), which reveals that the deposited tin in the Sn–O–C composite corresponds to the body center tetragonal phase of β-tin. The selected area electron diffraction (SAED) patterns of 'area 3' in Fig. 3(a) shows clear ring patterns which imply a polycrystalline Sn phase, as shown in Fig. 3(d). Therefore, the Sn–O–C composite contains a polycrystalline Sn phase, which consists of individual β-Sn single

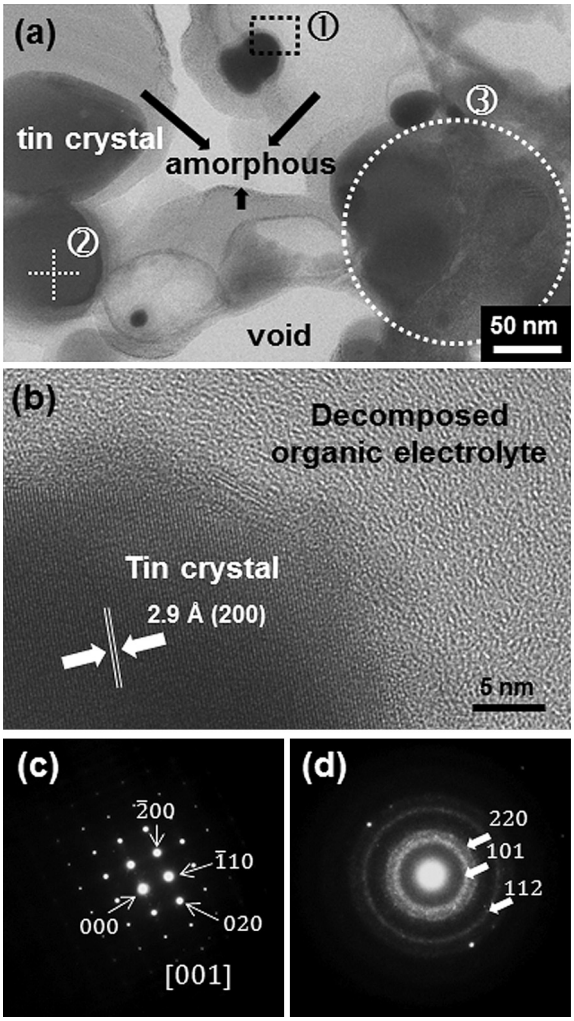

Fig. 3. (a) Cross-sectional TEM image of the as-prepared Sn–O–C composite material. (b) HR-TEM images of part 1 in (a). (c) FFT image of point 2 in (a), and (d) SAED pattern of area 3 in (a).

crystals coated by the decomposed products of an organic carbonate electrolyte. The inter-particle void space and the decomposed products of an organic electrolyte will effectively act as a buffer-enduring volume expansion.

Fig. 4 shows quantitative depth profiles for each element present in the as-deposited Sn–O–C composite. The presence of tin, carbon and oxygen is clearly seen in the GDOES depth profile. This result corresponds to our previous report on the Si–O–C composite anode, which was prepared by electrodeposition using a propylene

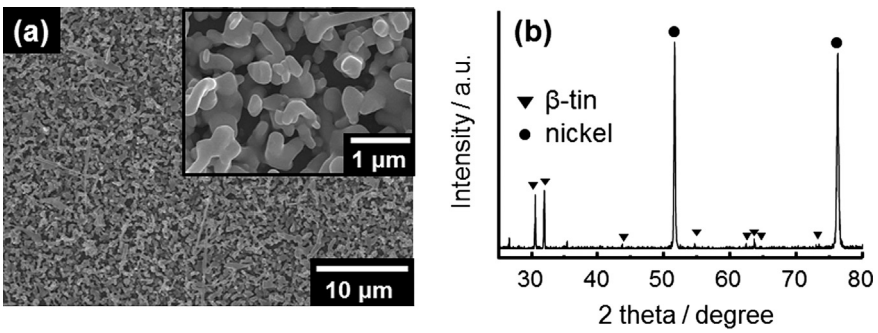

Fig. 2. Plane view FE-SEM images with different magnification (a). A XRD pattern (b) of the as-prepared Sn–O–C composite material.

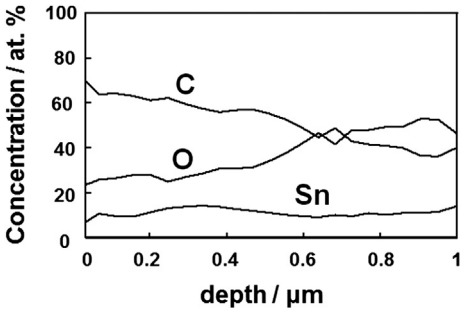

Fig. 4. GDOES depth profile of the as-prepared Sn–O–C composite material.

carbonate electrolyte [18]. In the previous work, we reported that the obtained carbon and oxygen of the GDOES depth profile were derived from the decomposition of the organic carbonate electrolyte during electrodeposition, which was proved by XPS analysis. In agreement with the result, it is assumed that carbon and oxygen existing in the Sn–O–C composite are the products of the decomposition of the organic carbonate electrolyte. The tin content is constant from the surface to the deposit–substrate interface. On the other hand, carbon and oxygen contents vary gradually with depth, *i.e.*, the oxygen content gradually rises with increase in depth showing ca. 25 at.% at the surface and ca. 47 at.% at the deposit–substrate interface, respectively. This is presumably attributable to the applied low over-potential at the beginning of the deposition process, *i.e.*, ca. 2.2 V, which results in an incomplete reduction of the Sn^{2+} ion during this process. Thus, it is assumed that greater amounts of SnO or SnO_2 remain nearer the deposit–substrate interface than on the surface, which is produced at the initial stages of the deposition process. Also, the result of the element composition corresponds to that measured by EDS analysis as discussed above. The averaged composition estimated by EDS analysis was obtained as C:O:Sn = 26.7:17.5:53.9 in weight.

The CVs of the as-deposited Sn–O–C composite anode recorded at the scan rate of 10 mV s^{-1} between 0.01 and 1 V are shown in Fig. 5(a). In the first cycle, three cathodic peaks at ca. 1.3, 0.6 and 0.3 V and four anodic peaks at 0.5, 0.65, 0.7 and 0.85 V are found for lithiation and delithiation, respectively. The cathodic peak found at 1.3 V originated from SEI formation on the surface of active particles. It is generally regarded that the charge/discharge reaction of the Sn anode occurs in multiple stages, which correspond to the following reactions of lithiation, and delithiation [21].

$$Sn \rightarrow Li_{0.4}Sn \text{ (at 0.6 V)} \rightarrow Li_{2.33}Sn \text{ (at 0.3 V)} \rightarrow Li_{4.4}Sn \text{ (a gradual decrease from 0.3 V to 0.1 V)}$$

$$Li_{4.4}Sn \rightarrow Li_{2.33}Sn \text{ (0.4 V)} \rightarrow LiSn \text{ (0.7 V)} \rightarrow Sn \text{ (0.8 V)}$$

The CVs of the Sn–O–C composite anode also clearly show several redox peaks which are related to the multi-stage reaction of lithiation/delithiation during cycling. The redox peaks are continuously obtained with successive cycles; however, the current slightly decreases with the cycle number. It represents that the reaction of lithiation and delithiation is not completely reversible although the multi-stage reaction is persistently carried out. The cathodic peaks that appeared around 0.4 V showed a small shift in the negative direction while the onset potential of the peaks did not. It was considered that the increase in resistance in the anode matrix during the potential cycling was due to the accumulation of the insulating product by the reduction of the Sn oxide and/or the electrolyte solvent.

Fig. 5(b) shows the electrochemical cycling performance measured by the galvanostatic charge/discharge test at the current

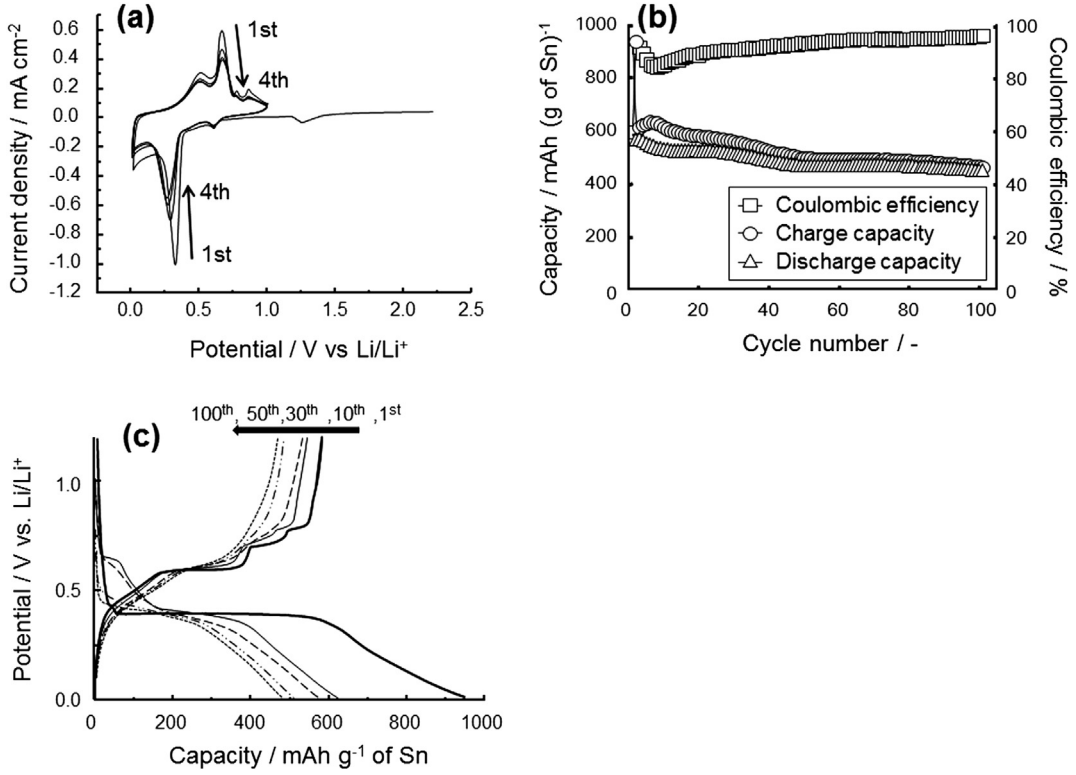

Fig. 5. Electrochemical performance of the Sn–O–C material. (a) Cyclic voltammograms measured between 0.01 and 1.0 V vs. Li/Li^+ at 10 mV s^{-1}. (b) Capacities of charge and discharge and coulombic efficiency during continuous constant current charge–discharge cycles. (c) Potential profiles during charge/discharge cycling at the 1st, 10th, 30th, 50th and 100th cycles.

Table 1
Capacity values and coulombic efficiency obtained during lithiation and delithiation at selected cycle numbers (the 1st, 10th, 50th and 100th) of the Sn–O–C composite anode.

	1st cycle	10th cycle	30th cycle	50th cycle	100th cycle
Charge capacity/mAh (g of Sn)$^{-1}$	950.7	621.0	570.2	511.7	477.4
Discharge capacity/mAh (g of Sn)$^{-1}$	582.2	543.5	527.2	483.4	465.6
Coulombic efficiency/%	61.2	87.5	92.4	94.5	97.5

density of 20 μA cm^{-2}, which corresponded to 0.16 C. The first cycle indicated a high charge and discharge capacity of 950 and 582 mAh g^{-1}, respectively, but a poor coulombic efficiency of 61%. The low coulombic efficiency at the first cycle of the electrodeposited composite anode was due to further reduction of the remaining oxide states of active material and SEI formation [17,18,26]. During the electrodeposition process, some of the Sn oxides were not completely reduced and remained in the oxide state. Therefore, the contribution of the reducing charge for the Sn oxide causes the abnormally low coulombic efficiency. After the first cycle in the following cycling, the charge capacity increased while the discharge capacity decreased for several cycles. This may be due to the irreversible formation of the SEI layer on the fresh surface appearing due to the cracking of the Sn–O–C layer during cycling, which was confirmed by SEM images of the Sn–O–C anode after several cycles (see Supplementary). Afterward, the constant value of the discharge capacity continued until the 30th cycle followed by the second region of a decrease in the discharge capacity up to the 50th cycle. It is assumed that the SEI layer is formed during the first period of decrease in discharge capacity, *i.e.*, from the 1st cycle to the 10th cycle, and then, the lithiation/delithiation reactions occurred stably up to ca. the 30th cycle. Simultaneously, a slight crack and pulverization on the surface of the Sn–O–C composite were found. As a result, the second region of the decrease in discharge capacity appeared. After the 50th cycle, stable cycle performance was achieved up to the 100th cycle without a further decrease in discharge capacity. The obtained capacity and coulombic efficiency at the selected cycle number are summarized in Table 1. A discharge capacity of 465 mAh (g of Sn)$^{-1}$/256 mAh (g of deposit)$^{-1}$ was obtained from the 100th cycle, showing 80% of the capacity retention compared with the value of the discharge capacity at the first cycle. The coulombic efficiency shows a value higher than 80% in overall charge/discharge cycling except for the first cycle, and even higher than 90% after the 50th cycle. The total efficiency for cycling from the 51st to the 100th was 96.3% calculated by the accumulative discharge capacity divided by the accumulative charge of 50 cycling with an accumulative irreversible capacity of 913 mAh (g of Sn)$^{-1}$. The irreversible capacity would be reduced by selecting an adequate additive to the electrolyte solution, while in this work no additives were introduced.

Fig. 5(c) shows potential profiles during the charge/discharge test of the Sn–O–C composite anode with a voltage range between 0.01 and 1.2 V vs. Li/Li$^+$. In the first charge process the rapid potential drop to 0.4 V occurred with a large plateau followed by a gradual potential decease to 0.01 V. The initial potential drop of the first cycle revealed that in the first cycle on Sn–O–C, the reduction current was not used to form the SEI film as reported in previous literature [25,27,28]. The small plateaus around 0.6 V were observed during the charging process of the 10th and 30th cycles, but not observed after the 30th cycle, which may indicate the formation of $Li_{0.4}Sn$ and/or the reduction of the electrolyte to form the SEI film on the fresh interface created by cracking. The second plateau regions around 0.3 V and the gradual decreases in potential toward 0.1 V appear at these cycles corresponding to the indication of the lithiation process of $Li_{2.33}Sn$ and $Li_{4.4}Sn$, respectively. During the charge process of the 50th and 100th cycles, the small plateau region around 0.6 V disappeared and the potential started to drop immediately to the plateau region at 0.3 V. These tendencies were observed during the discharge process as well. In other words, four plateau regions at ca. 0.4, 0.6, 0.7 and 0.8 V attributing to the delithiation process are clearly distinguishable at the 1st and the 10th cycles, while smooth potential curves were shown at the 30th, 50th and 100th cycles. It is assumed that the formation of the lithium-tin alloy phase (lithiation) and its dealloying (delithiation) reactions reversibly occur during the initial 10 cycles. Afterward, the alloys of Sn and Li started to be oxidized up to $Li_{0.4}Sn$ instead of Sn at the discharged state.

Differential capacity curves with selected cycle numbers are illustrated in Fig. 6 to validate the phase transformation of the $Li_{0.4}Sn$ of the Sn–O–C composite anode with cycling. The differential capacity curves during the charge and discharge processes for the 1st, 10th, 30th and 50th cycles are shown in Fig. 6(a) and (b), respectively. Small and large sharp peaks at ca. 0.4, 0.43 and 0.65 V for lithiation and 0.46, 0.6, 0.7 and 0.78 V for delithiation are obtained at the 1st and 10th cycles of charge/discharge cycling. However, after the 30th cycle, the sharp peaks changed to broad peaks, *i.e.*, at 0.4 and 0.63 V for lithiation and 0.46, 0.6, 0.7 and 0.78 V for delithiation, and the peak height was also decreased in comparison to those at the former cycles. These behaviors indicate a fading of the capacity with cycling. All the peaks corresponding to the multi-stage reaction of lithiation/delithiation are achieved with slight alteration in the 1st, 10th, and 30th cycles; on the other hand,

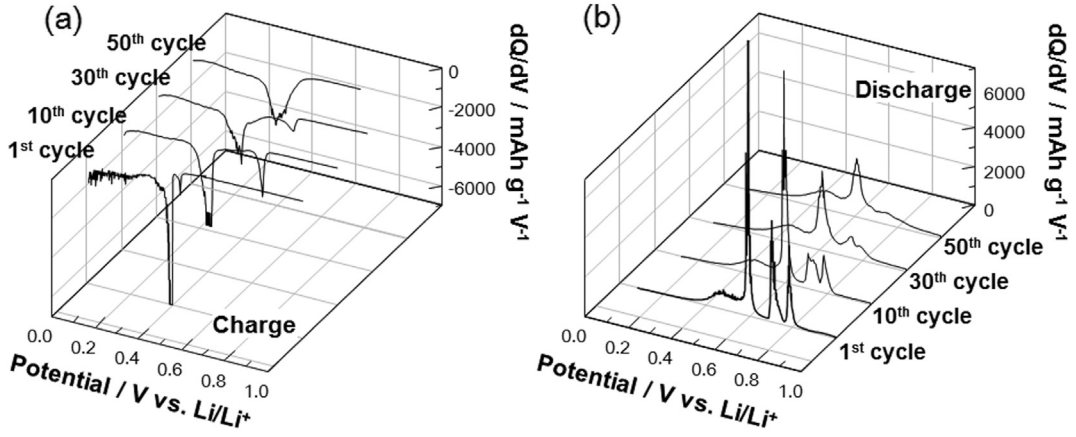

Fig. 6. Differential capacity curves of the Sn–O–C composite anode at selected cycle numbers (1st, 10th, 30th and 50th cycles) during the charge (a) and discharge (b) process.

the peaks at 0.6 V for lithiation and 0.8 V for delithiation, which are corresponding to the reaction between $Li_{0.4}Sn$ and Sn, disappears in the differential capacity curve at the 50th cycle. This tendency corresponds well to the result of the potential profile.

4. Conclusion

In summary, a Sn–O–C composite anode was synthesized by an electrodeposition method using an organic carbonate electrolyte. Tin reduction and decomposition of an organic carbonate electrolyte simultaneously occurred during the electrodeposition. It is thus assumed that the decomposition product of an organic electrolyte, similar to the compound of the SEI layer on the anode in Lithium ion batteries, embed the crystalline tin deposits. EDS and GDOES results revealed the consistent composition of tin, oxygen and carbon of the composite. The electrochemical investigation exhibited Sn–O–C has potential as an anode of a lithium secondary battery with the discharge capacity of more than 450 mAh (g of Sn)$^{-1}$ at the 100th charge discharge cycle.

Acknowledgments

This work was partly supported by a Grant-in-Aid for specially promoted research “Establishment of electrochemical device engineering” from the Ministry of Education, Culture, Sports, Science and Technology (MEXT), Japan, “Research & Development Initiative for Scientific Innovation of New Generation Batteries” from New Energy and Industrial Technology Development Organization (NEDO), Japan, and was partly done in the Global COE Program “Center for Practical Wisdom” and Grants for Excellent Graduate Schools (Practical Chemical Wisdom), from MEXT, Japan.

Appendix A. Supplementary data

Supplementary data related to this article can be found at http://dx.doi.org/10.1016/j.jpowsour.2013.05.136.

References

[1] R. Hu, M. Zeng, C. Li, M. Zhu, J. Power Sources 188 (2009) 268.
[2] L. Ji, Z. Tan, T. Kuykendall, E.J. An, Y. Fu, V. Battaglia, Y. Zhang, Energy Environ. Sci. 4 (2011) 3611–3616.
[3] S. Brutti, J. Hassoun, B. Scrosati, C. Lin, H. Hsieh, J. Power Sources 217 (2012) 72.
[4] F. Ke, L. Huang, B.C. Solomon, G. Wei, L. Xue, B. Zhang, J. Li, X. Zhou, S. Sun, J. Mater. Chem. 22 (2012) 17511.
[5] Z. Du, S. Zhang, Y. Xing, X. Wu, J. Power Sources 196 (2011) 9780.
[6] Y. Lee, Y. Kang, J. Power Sources 196 (2011) 10686.
[7] H. Mukaibo, T. Sumi, T. Yokoshima, T. Momma, T. Osaka, Electrochem. Solid-State Lett. 6 (2003) A218.
[8] H. Mukaibo, T. Momma, M. Mohamedi, T. Osaka, J. Electrochem. Soc. 152 (2005) A560.
[9] Z. Chen, Y. Cao, J. Qian, X. Ai, H. Yang, J. Mater. Chem. 20 (2010) 7266.
[10] G. Derrien, J. Hassoun, S. Panero, B. Scrosati, Adv. Mater. 19 (2007) 2336.
[11] K.T. Lee, Y.S. Jung, Seung M. Oh, J. Am. Chem. Soc. 125 (2003) 5652.
[12] X.W. Lou, Y. Wang, C.L. Yuan, J.Y. Lee, L.A. Archer, Adv. Mater. 18 (2006) 2325.
[13] I. Grigoriants, B. Markovsky, R. Persky, I. Perelshtein, A. Gedanken, D. Aurbach, B. Filanovsky, T. Bourenko, Israel Felner, Electrochim. Acta 54 (2008) 690.
[14] H. Nara, Y. Fukuhara, A. Takai, M. Komatsu, H. Mukaibo, Y. Yamauchi, T. Momma, K. Kuroda, T. Osaka, Chem. Lett. 37 (2008) 142.
[15] Y. Xu, J. Guo, C. Wang, J. Mater. Chem. 22((2012) 9562.
[16] Y. Zhou, C. Jo, J. Lee, C. Lee, G. Qao, S. Yoon, Microporous Mesoporous Mater. 151 (2012) 172.
[17] T. Momma, S. Aoki, H. Nara, T. Yokoshima, T. Osaka, Electrochem. Commun. 13 (2011) 969.
[18] H. Nara, T. Yokoshima, T. Momma, T. Osaka, Energy Environ. Sci. 5 (2012) 6500.
[19] J. Chen, S.J. Bull, S. Roy, H. Mukaibo, H. Nara, T. Momma, T. Osaka, Y. Shacham-Diamand, J. Phys. D Appl. Phys. 41 (2008) 1.
[20] N. Tamura, R. Ohshita, M. Fujimoto, S. Fujitani, M. Kamino, I. Yonezu, J. Power Sources 107 (2002) 48.
[21] D.H. Nam, R.H. Kim, D.W. Han, H.S. Kwon, Electrochim. Acta 66 (2012) 126.
[22] C. Li, W. Ho, C. Jiang, C. Lai, M. Wang, S. Yen, J. Power Sources 196 (2011) 768.
[23] J. Park, J. Eom, H. Kwon, Electrochem. Commun. 11 (2009) 596.
[24] X. Chen, J. Guo, K. Gerasopoulos, A. Langrock, A. Brown, R. Ghodssi, J.N. Culver, C. Wang, J. Power Sources 211 (2012) 129.
[25] I.T. Lucas, J. Syzdek, R. Kostecki, Electrochem. Commun. 13 (2011) 1217.
[26] D. Aurbach, A. Nimberger, B. Markovsky, E. Levi, E. Sominski, A. Gedanken, Chem. Mater. 14 (2002) 4155.
[27] L.Y. Beaulieu, T.D. Hatchard, A. Bonakdarpour, M.D. Fleischauer, J.R. Dahn, J. Electrochem. Soc. 150 (2003) A1457.
[28] J. Bridel, S. Grugeon, S. Laruellea, J. Hassoun, P. Reale, B. Scrosati, J. Tarascon, J. Power Sources 195 (2010) 2036.